Electronic Supplementary Material (ESI) for New Journal of Chemistry.

Multifunctionality and size of the chloranilate ligand define the topology of transition metal coordination polymers

Supporting Information

Lidija Androš Dubraja,[a] Krešimir Molčanov,*[a] Dijana Žilić,[a] Biserka Kojić-Prodić,[a] Emmanuel Wenger[b]

[a] Rudjer Bošković Institute, Bijenička 54, Zagreb HR-10000, Croatia

[b] Cristallographie, Résonance Magnétique et Modélisations CNRS, UMR 7036, Institut Jean Barriol, CNRS and Université de Lorraine BP 70239, F54506 Vandoeuvre-lès-Nancy CEDEX, France

e-mail: kmolcano@irb.hr

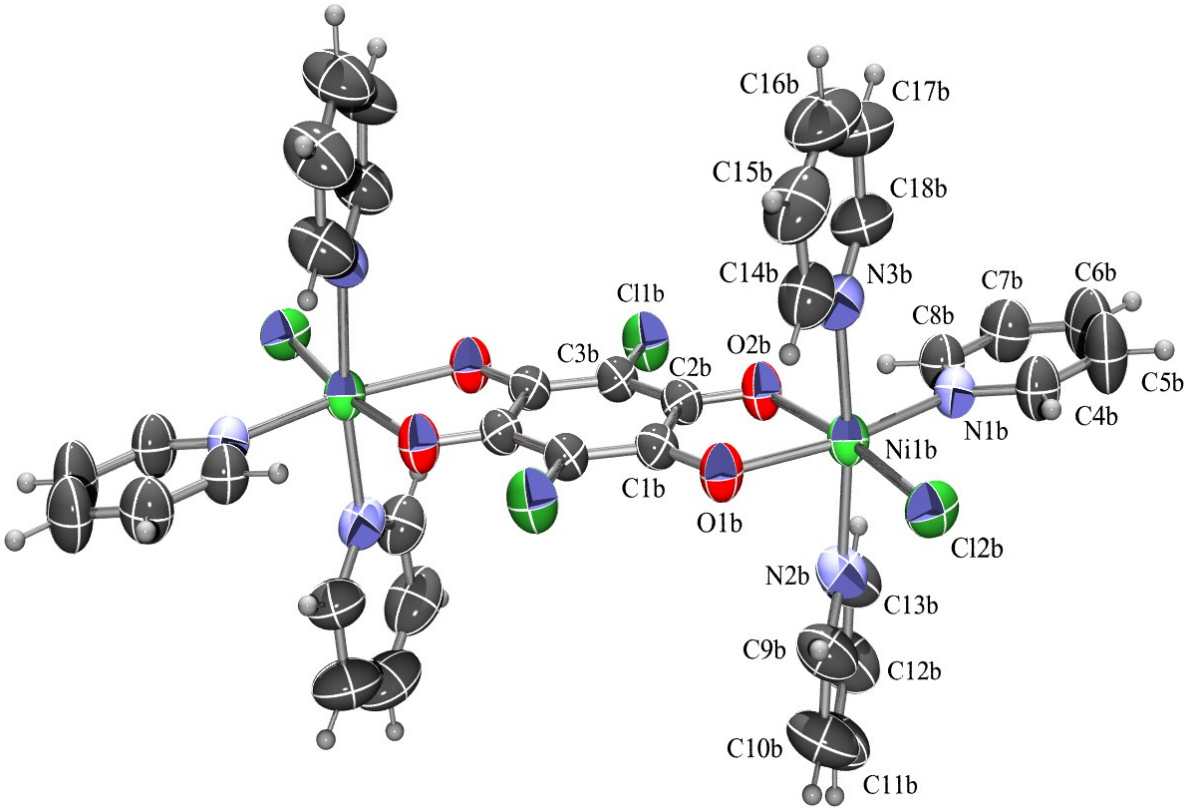

Figure S1 ORTEP-3 [1] drawing of **4** (molecule b; crystallographic inversion centre is located in the centroid of the chloranilate ring). Displacement ellipsoids are drawn for the probability of 50 % and hydrogen atoms are shown as spheres of arbitrary radii.

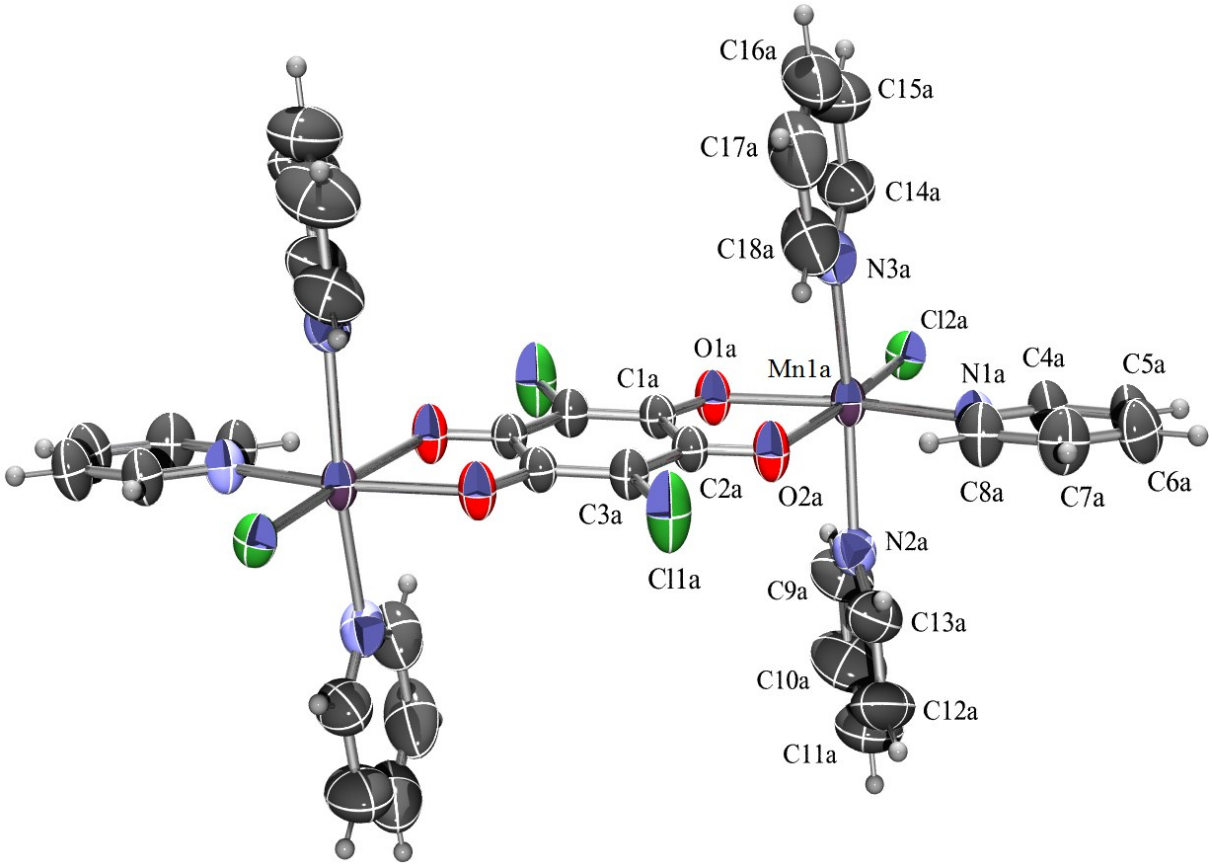

Figure S2 ORTEP-3 [1] drawing of **5** (molecule A; crystallographic inversion centre is located in the centroid of the chloranilate ring). Displacement ellipsoids are drawn for the probability of 50 % and hydrogen atoms are shown as spheres of arbitrary radii.

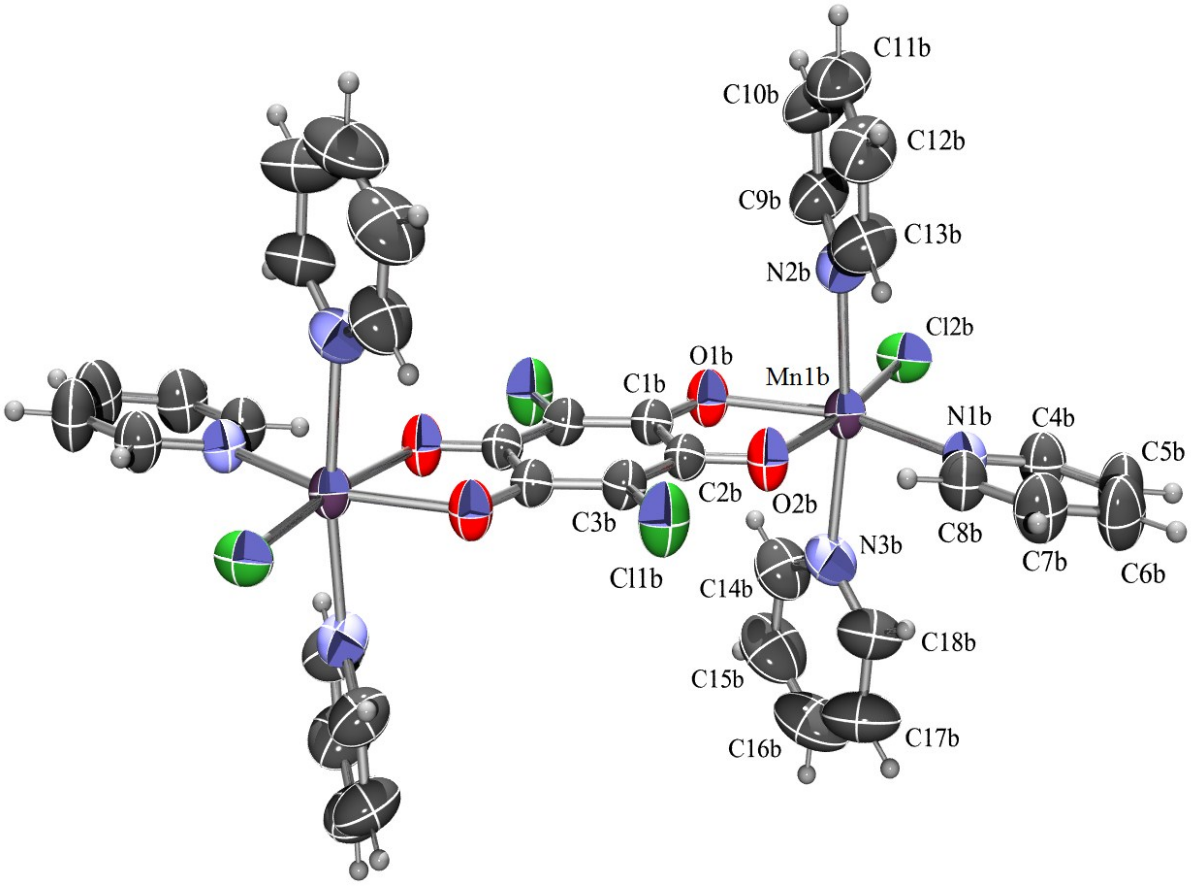

Figure S3 ORTEP-3 [1] drawing of **5** (molecule B; crystallographic inversion centre is located in the centroid of the chloranilate ring). Displacement ellipsoids are drawn for the probability of 50 % and hydrogen atoms are shown as spheres of arbitrary radii.

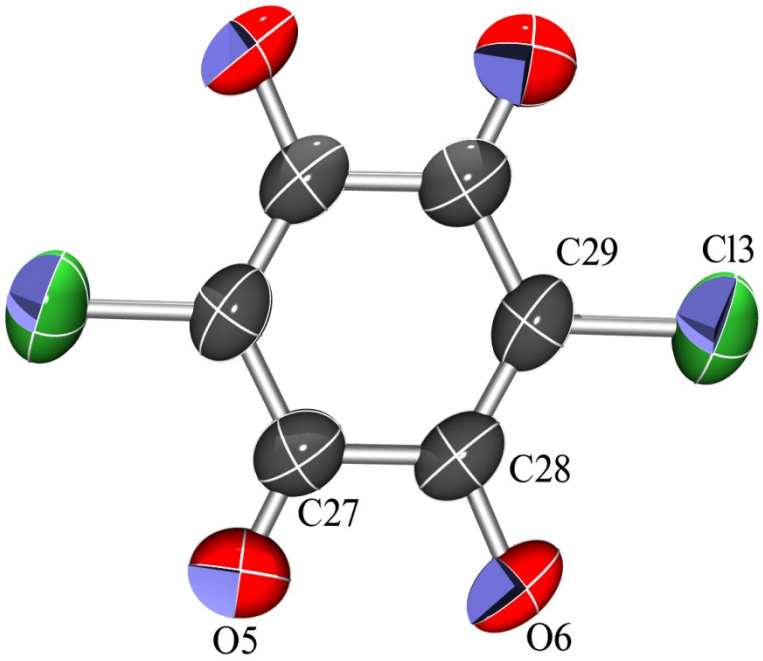

Figure S4 ORTEP-3 [1] drawing of the chloranilate dianion from **3** with atom numbering scheme. Displacement ellipsoids are drawn for the probability of 50 % and hydrogen atoms are shown as spheres of arbitrary radii.

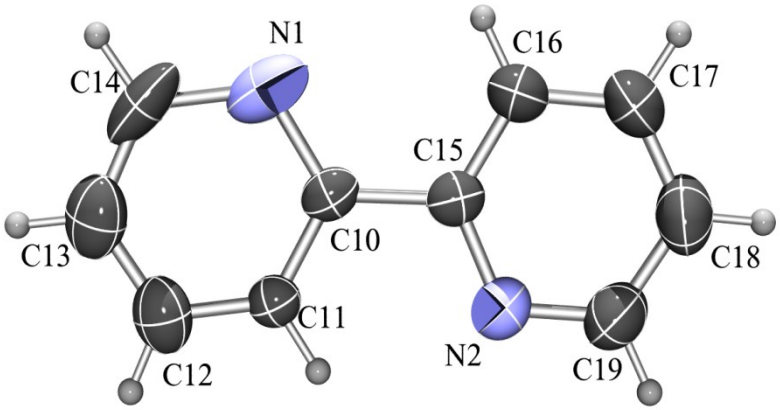

Figure S5 ORTEP-3 [1] drawing of the bipyridium cation from **8**. Displacement ellipsoids are drawn for the probability of 50 % and hydrogen atoms are shown as spheres of arbitrary radii.

Table S1 Geometric parameters of the metal coordination spheres.

	1		**2**		**3**
Ni1 – O1	2.0579(15)	Ni1 – O2	2.064(17)	Cr1 – O2	1.9434(18)
		Ni1 – O1	2.052(19)	Cr1 – O1	1.9459(17)
Ni1 – N2	2.0702(17)	Ni1 – N1	2.09(2)	Cr1 – N1	2.058(2)
		Ni1 – N4	2.06(2)	Cr1 – N4	2.059(2)
Ni1 – N1	2.0912(18)	Ni1 – N3	2.08(2)	Cr1 – N3	2.061(2)
		Ni1 – N2	2.08(2)	Cr1 – N2	2.070(2)
O1 – Ni1 – O1^{i}	79.81(6)	O2 – Ni1 – O1	79.4(7)	O2 – Cr1 – O1	82.81(7)
O1 – Ni1 – N2	92.50(6)	O2 – Ni1 – N1	89.9(8)	O2 – Cr1 – N1	97.64(9)
O1 – Ni1 – N2^{i}	91.57(6)	O2 – Ni1 – N4	95.8(8)	O2 – Cr1 – N4	92.23(9)
O1 – Ni1 – N1	93.54(6)	O2 – Ni1 – N3	169.5(8)	O2 – Cr1 – N3	92.88(8)
O1 – Ni1 – N1^{i}	169.16(6)	O2 – Ni1 – N2	95.3(8)	O2 – Cr1 – N2	175.74(9)
		O1 – Ni1 – N1	94.7(9)	O1 – Cr1 – N1	91.85(8)
		O1 – Ni1 – N4	92.5(8)	O1 – Cr1 – N4	94.63(9)
		O1 – Ni1 – N3	91.7(8)	O1 – Cr1 – N3	172.19(9)
		O1 – Ni1 – N2	171.7(8)	O1 – Cr1 – N2	94.71(8)
N2 – Ni1 – N2^{i}	174.71(7)	N1 – Ni1 – N4	171.6(9)	N1 – Cr1 – N4	168.80(9)
N2 – Ni1 – N1	80.11(7)	N1 – Ni1 – N3	96.4(8)	N1 – Cr1 – N3	95.19(9)
N2 – Ni1 – N1^{i}	96.25(7)	N1 – Ni1 – N2	78.9(9)	N1 – Cr1 – N2	78.93(9)
		N4 – Ni1 – N3	79.0(8)	N4 – Cr1 – N3	78.98(9)
		N4 – Ni1 – N2	94.3(9)	N4 – Cr1 – N2	91.43(9)
N1 – Ni1 – N1^{i}	94.26(7)	N3 – Ni1 – N2	94.2(8)	N3 – Cr1 – N2	89.98(9)

	4a	**4b**	**5a**	**5b**
M1* – O2	2.0832(14)	2.0721(15)	2.2126(15)	2.2178(16)
M1* – N1	2.1041(15)	2.0914(19)	2.2616(16)	2.2551(19)
M1* – N2	2.127(2)	2.146(2)	2.302(2)	2.322(2)
M1* – O1	2.1305(12)	2.1061(16)	2.2362(14)	2.2239(17)
M1* – N3	2.146(2)	2.142(2)	2.310(2)	2.338(2)
M1* – Cl2	2.3832(6)	2.3537(6)	2.4227(6)	2.3992(7)
O2 – M1* – N1	93.77(6)	90.48(7)	91.89(6)	85.25(7)
O2 – M1* – N2	85.94(6)	86.98(7)	83.89(7)	85.75(7)
O2 – M1* – O1	77.27(5)	78.29(6)	72.73(5)	72.79(6)
O2 – M1* – N3	89.25(7)	89.09(7)	85.53(7)	88.13(7)
O2 – M1* – Cl2	170.20(4)	170.88(5)	170.02(4)	171.44(5)
N1 – M1* – N2	90.69(7)	93.75(8)	88.89(7)	93.22(7)
N1 – M1* – O1	170.98(6)	168.53(7)	164.57(6)	157.75(7)
N1 – M1* – N3	89.16(7)	91.14(8)	88.52(7	90.49(8)
N1 – M1* – Cl2	95.38(5)	98.61(5)	97.79(5)	103.15(5)
N2 – M1* – O1	89.72(6)	88.04(7)	90.54(6)	88.73(7)

N2 – M1* – N3	175.17(7)	173.75(8)	169.01(7)	172.55(7)	
N2 – M1* – Cl2	90.43(5)	91.61(5)	93.82(5)	92.07(5)	
O1 – M1* – N3	89.68(6)	86.41(7)	89.13(6)	85.41(7)	
O1 – M1* – Cl2	93.63(4)	92.67(4)	97.63(4)	98.92(5)	
N3 – M1* – Cl2	94.39(5)	91.51(5)	97.10(5)	93.38(6)	
	8		**6**		**7**
Mn1 – O4	2.1452(19)	Co2 – O2	2.0725(18)	Mn1 – O2	2.168(2)
Mn1 – O7	2.153(2)			Mn1 – O1	2.186(2)
Mn1 – O2	2.181(2)	Co2 – O1	2.096(2)	Mn1 – O3	2.188(2)
Mn1 – O6	2.182(2)			Mn1 – O4	2.189(2)
Mn1 – O5	2.217(2)	Co2 – N1	2.108(3)	Mn1 – N2	2.243(3)
Mn1 – O1	2.2378(18)			Mn1 – N1	2.245(3)
O4 – Mn1 – O7	86.95(9)	O2 – Co1 – O2^{ii}	158.86(10)	O2 – Mn1 – O1	73.80(9)
O4 – Mn1 – O2	89.82(7)	O2 – Co1 – O1	77.78(8)	O2 – Mn1 – O3	92.01(9)
O4 – Mn1 – O6	115.75(9)	O2 – Co1 – O1^{ii}	88.85(8)	O2 – Mn1 – O4	103.34(9)
O4 – Mn1 – O5	86.34(9)	O2 – Co1 – N1	94.62(9)	O2 – Mn1 – N2	103.35(9)
O4 – Mn1 – O1	162.23(8)	O2 – Co1 – N1^{ii}	101.82(9)	O2 – Mn1 – N1	154.63(10)
O7 – Mn1 – O2	103.67(8)	O2^{ii} – Co1 – O1	88.85(8)	O1 – Mn1 – O3	158.60(9)
O7 – Mn1 – O6	92.43(8)			O1 – Mn1 – O4	94.20(9)
O7 – Mn1 – O5	160.22(9)			O1 – Mn1 – N2	115.29(10)
O7 – Mn1 – O1	96.06(9)			O1 – Mn1 – N1	84.74(9)
O2 – Mn1 – O6	150.66(8)	O1^{ii} – Co1 – O1	101.64(9)	O3 – Mn1 – O4	73.19(9)
O2 – Mn1 – O5	94.91(8)	O1^{ii} – Co1 – N1	90.96(9)	O3 – Mn1 – N2	83.14(10)
O2 – Mn1 – O1	72.44(7)	O1^{ii} – Co1 – N1^{ii}	165.03(9)	O3 – Mn1 – N1	112.19(10)
O6 – Mn1 – O5	73.88(8)			O4 – Mn1 – N2	144.66(10)
O6 – Mn1 – O1	81.70(9)			O4 – Mn1 – N1	91.36(10)
O5 – Mn1 – O1	95.99(9)	N1^{ii} – Co1 – N1	77.86(10)	N2 – Mn1 – N1	73.49(10)

***** In two isostructural compounds **4** and **5** M denotes Ni and Mn, respectively.

Symmetry operators: *i*) –*x*, *y*, 1/2 – *z*; *ii*) 1–*x*, *y*, 3/2 – *z*.

Table S2 Geometric parameters of the π-interactions. Symmetry operators: *i*) x, 1+y, z; *ii*) x, –1+y, z; *iii*) 1–x, y, 3/2–z.

$\pi\cdots\pi$	Cg[a]···Cg / Å	α[b]	β[c]	Cg···plane(Cg2) / Å	Offset/ Å[d]	Symm. op. on Cg2
1						
N1→C8···N1→C8	3.9013(14)	0.03(12)	27.9	3.4474(10)	1.826	-–x, –y, 1–z
N1→C8···C7→C14	3.6176(15)	1.83(12)	19.4	3.4433(10)	1,20[d]	–x, –y, 1–z
2						
N2→C16···N2→C16	3.745(16)	0	23.8	3.426(11)	1.511	1–x, 2–y, 1–z
N4→C26···N4→C26	3.622(17)	1	20.1	3.422(13)	1.24[d]	–x, 1–y, –z
3						
N1→C11···N1→C11	3.7752(16)	0.02(13)	23.0	3.4762(11)	1.472	1–x, 1–y, 1–z
N3→C21···N4→C26	3.7105(19)	3.77(16)	26.6	3.4155(14)	1.54d	2–x, 2–y, –z
C1→C6···C1→C6	3.6743(14)	0.03(11)	27.6	3.2553(10)	1.704	1–x, 2–y, 1–z
4						
N2A→C13A···N3B→C18B	3.933(2)	6.81(17)	21.6	3.4678(15)	-	x, y, z
N2A→C13A···N3B→C13B	4.1687(18)	10.40(16)	23.9	3.7856(15)	-	–x, –1–y, –z
5						
N2A→C13A···N3B→C18B	4.038(2)	11.1(2)	17.0	3.5788(18)	-	x, y, z
N2A→C13A···N3B→C13B	4.164(2)	16.52(18)	25.0	3.8993(18)	-	–x, –1–y, –z
6						
Co1→N1[iii]···N1→C8	4.004(2)	2.44(16)	27.4	3.4848(12)	1.84[d]	1–x, 1–y, 1–z
N1→C8···N1→C8	4.123(3)	0.00(19)	31.4	3.5193(16)	2.148	1–x, 1–y, 1–z
N1→C8···N1→C8	4.305(2)	4.04(19)	35.2	3.5798(16)	2.48[d]	x, 1–y, –1/2+z
7						
Mn1→O2···C10→C17	3.807(2)	2.18(17)	26.1	3.4701(12)	1.67[d]	–x, –y, 1–z
N1→C11···N1→C11	3.543(3)	1.0(2)	5.5	3.527(2)	0.34[d]	1/2–x, y, 1–z
N1→C11···N2→C16	3.875(3)	1.8(2)	27.4	3.482(2)	1.78[d]	–x, –y, 1–z
N1→C11···C10→C17	4.038(3)	1.1(2)	31.5	3.471(2)	2.11[d]	–x, –y, 1–z
N2→C16···C10→C17	4.076(3)	0.8(2)	32.8	3.447(2)	2.21[d]	–x, –y, 1–z
C10→C17··· C10→C17	3.618(2)	1.0(2)	13.0	3.5247(17)	0.81[d]	1/2–x, y, 1–z
C10→C17··· C10→C17	3.527(2)	0.0(2)	12.1	3.4491(17)	0.738	–x, –y, 1–z
8						
Mn1→O2···Mn1→O2	4.0397(14)	0.50(11)	28.9	3.5361(10)	1.95[d]	3/2–x, y, 3/2–z
Mn1→O2···C1→C6[i]	4.2187(15)	3.65(12)	34.3	3.4867(10)	2.38[d]	3/2–x, y, 3/2–z
Mn1→O2···C4→C3[ii]	4.2187(15)	3.65(12)	34.3	3.4867(10)	2.38[d]	3/2–x, 1+y, 3/2–z
C1→C6[i] ···C1→C6[i]	3.4306(17)	4.33(13)	8.6	3.3920(12)	0.51[d]	3/2–x, y, 3/2–z
C1→C6[i]···C4→C3[ii]	3.4306(17)	4.33(13)	8.6	3.3920(12)	0.51[d]	3/2–x, 1+y, 3/2–z
C4→C3[ii]···C4→C3[ii]	3.4306(17)	4.33(13)	8.6	3.3920(12)	0.51[d]	3/2–x, y, 3/2–z

C4→C3^{ii}···N2→C19	3.783(2)	13.74(19)	13.4	3.4617(12)	-	*x*, *y*, *z*
C1→C6^{i}···N2→C19	3.783(2)	13.74(19)	13.4	3.4617(12)	-	*x*, 1+*y*, *z*

[a] Cg = centre of gravity of the aromatic ring.

[b] α = angle between planes of two interacting rings.

[c] β = angle between Cg···Cg line and normal to the plane of the first interacting ring.

[d] Offset can be calculated only for the strictly parallel rings (α = 0.00°). For slightly inclined rings (α ≤ 5°) an approximate value is given.

Table S3 Geometric parameters of hydrogen bonds.

	D–H / Å	H···*A* / Å	*D*···*A* / Å	*D*–H···*A* / º	Symm. op. on *A*
3					
O7–H7A···O5	0.95(4)	2.42(7)	3.125(6)	132(7)	*x*, *y*, *z*
O7–H7A···O6	0.95(4)	1.90(6)	2.785(5)	154(8)	*x*, *y*, *z*
O7–H7B···O4	0.93(2)	1.99(3)	2.884(4)	161(8)	*x*, *y*, –1+*z*
2					
O5–H5A···O3	0.8(5)	2.6(5)	3.32(4)	149(10)	*x*, *y*, *z*
O5–H5A···O4	0.8(5)	2.2(6)	2.89(4)	140(10)	*x*, *y*, *z*
O5–H5B···O3	0.8(8)	2.1(5)	2.90(4)	169(10)	2–*x*, 1–*y*, 1–*z*
4					
C5B–H5B···Cl2B	0.93	2.73	3.617(3)	161	–*x*, –1–*y*, 1–*z*
C7B–H7B···Cl2A	0.93	2.71	3.630(3)	170	*x*, –1+*y*, *z*
C6B–H7B···Cl1A	0.93	3.11	3.852	139	1–*x*, –1–*y*, 1–*z*
C7A–H8A···Cl1A	0.93	3.13	3.725	124	1+*x*, *y*, *z*
C8A–H8A···Cl1A	0.93	2.98	3.667	132	*x*, *y*, *z*
8					
O7–H7A···O3	0.94(3)	1.86(3)	2.752(3)	159(5)	3/2–*x*, *y*, 3/2–*z*
O7–H7A···O4	0.94(3)	2.60(4)	3.231(3)	125(3)	3/2–*x*, *y*, 3/2–*z*
O7–H7B···O2	0.93(4)	1.82(4)	2.749(3)	173(4)	3/2–*x*, *y*, 3/2–*z*
O8–H8A···O1	0.95(6)	2.13(4)	2.956(5)	145(6)	*x*, –1+*y*, *z*
O8–H8B···O6	0.94(8)	2.23(8)	3.011(5)	140(7)	*x*, –1+*y*, *z*
O8–H8A···Cl2	0.95(6)	2.88(8)	3.628(5)	136(6)	*x*, –1+*y*, *z*
O8–H8B···Cl3	0.94(8)	2.85(8)	3.699(5)	150(7)	*x*, –1+*y*, *z*
N1···O8[a]	-	.	3.369(5)	-	1+*x*, *y*, *z*
N2···O5[a]	-	-	3.371(6)	-	*x*, *y*, *z*
N2···Cl3[a]	-	-	3.334(4)	-	1–*x*, –*y*, 1–*z*

a Possible hydrogen bonds, but hydrogen position could not be determined.

Magnetic properties

All Ni(II) complexes (**1**, **2** and **4**) were ESR silent in the whole investigated temperature range 78-296 K. Non-detecting spectra of Ni(II) with $S = 1$ at the X-band frequency could be assigned to a high value of its zero-field splitting (ZFS) parameter (parameter D) related to distorted octahedral coordination of Ni(II) ions in all investigated complexes (Table 1). Beside distortion of Ni(II) octahedra and existence of parameter D, an additional cause of non-observation spectra could be related to spin-relaxation phenomena. Furthermore, the similar situation is with **6** complex, where ESR signal of Co(II) ions with $S = 3/2$ was also not detected from room temperature down to 77 K. [2-4] In all Ni(II) complexes as well as in the Co(II) complex **6**, metal-metal distances are larger than 7.5 Å, which are quite large for observing significant magnetic interactions. [5]

The ESR spectra of polycrystalline sample of the compound **3**, at different temperatures, are shown in Fig. S6. The narrow signals marked with asterisks (at magnetic fields ~ 175, 334, 360, 396 and 420 mT) originate from ESR cavity. In accord with previous detailed single crystal [4,6] and high field/frequency HF-ESR powder studies [7] of similar class of Cr(III) compounds, the most prominent, broad line in the spectra in Fig. S6 is expected to be associated with the polycrystalline spectra of Cr(III) ion with the spin $S = 3/2$. Intensity of the line paramagnetically grows with decreasing temperature, indicating negligible interaction between Cr(III) ions. This is in agreement with the crystal structure of the investigated compound and the nearest Cr···Cr distance of 7.71 Å. The observed ESR signal corresponds to the allowed transition $M_S = -1/2 \leftrightarrow +1/2$. [2,7] Insert in Fig. S6 shows comparison of experimental spectrum with simulated spectrum of complex **6** at $T = 80$ K. The simulation was performed by *EasySpin* software, [8] using the following spin-Hamiltonian parameters: $g = 1.98$, $|D| = 25$ GHz and $E = 0$.

Fig. S8 shows ESR spectra of polycrystalline samples of compounds **5**, **7** and **8** at different temperatures. ESR spectra show one main line for all Mn(II) complexes in all investigated temperature range. This line with g-value $g \approx 2.02$ is characteristic for high spin Mn(II) ions with $S = 5/2$. [9] Linewidth and intensity of the line grows with decreasing of the temperature. For **7** and **8** and, the observed line was Lorentzian-like, while for **5**, the observed line was composed of two lines, that could be possible related to two magnetically nonequivalent Mn(II) ions in asymetric unit. This is consistent with presence of two symmetry-independent molecules in the crystal structure. For **5** and **8** complexes, no hyperfine lines due to interaction of electron spin with nuclear spin $I = 5/2$ were detected.

However, for the complex **7** characteristic six line pattern could be noticed at room temperature. Inserts in Fig. S7c present enlarged spectrum of **7** at RT and its derivative, respectively, where hyperfine sextet could be clearly seen. The observed almost equidistant peak-to-peak separation is around 9 mT, in agrrement with the similar values found for Mn(II) ions in literature. [9,10]

The featureless character (no hyperfine peaks) as well as Lorentzian-like ESR line for **8** complex reveal the presence of an exchange interaction stronger than the hyperfine interaction ($|J| \gg A$) for Mn(II) ions. [11,12] The observation of exchange coupling between Mn(II) ions in **8** is in agreement with the nearest Mn···Mn distance of 4.81 Å (in the neighbouring chains; the shortest intra-chain Mn···Mn distance exceeds 8.2 Å), contrary to quite larger intermetal distances in other two investigated Mn(II) complexes (more than 7.8 Å).

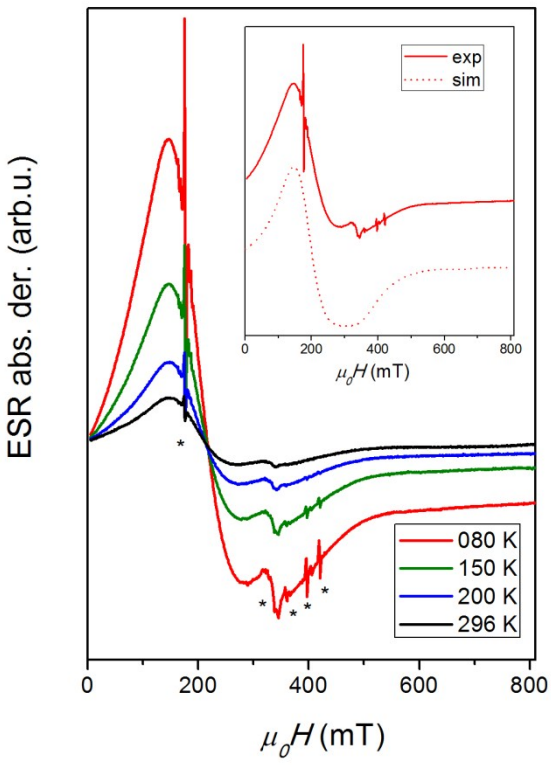

Figure S6 ESR spectra of polycrystalline samples of **3** complex at indicated temperatures. Inset shows experimental (solid line) and simulated spectrum (dotted line) at 80 K. The spin-Hamiltonian parameters used in the simulation are given in the text.

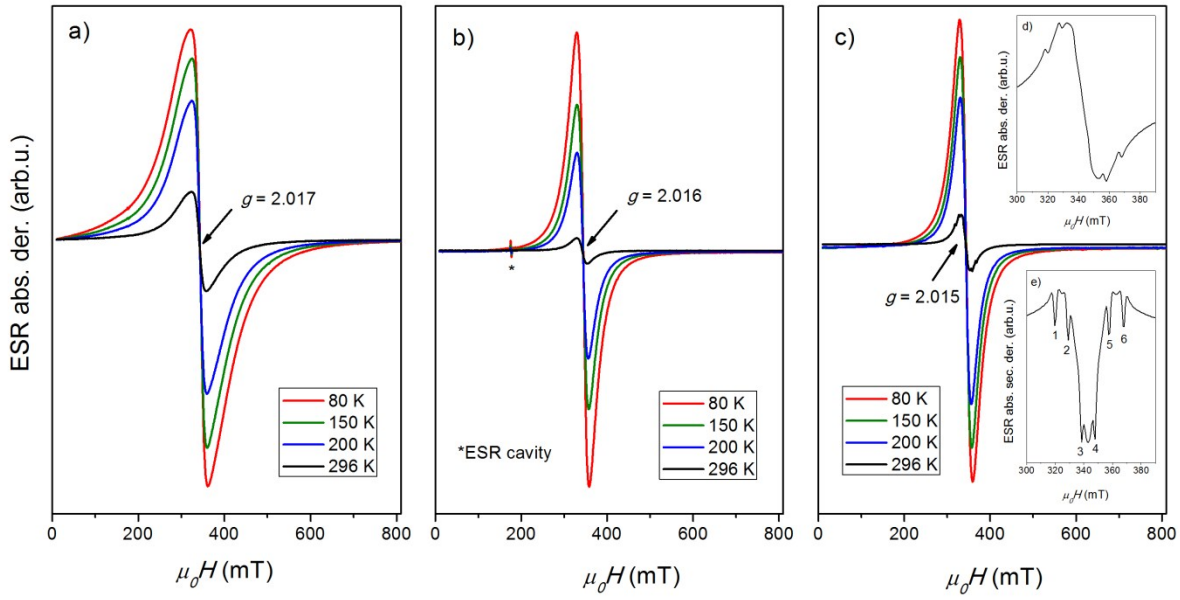

Figure S7 ESR spectra of polycrystalline samples of a) **5**, b) **8** and c) **7** complexes at indicated temperatures. Inserts d) and e) show enlarged spectrum of **7** complex at 296 K and its derivative with labeled Mn(II) hyperfine sextet lines, respectively.

IR spectra

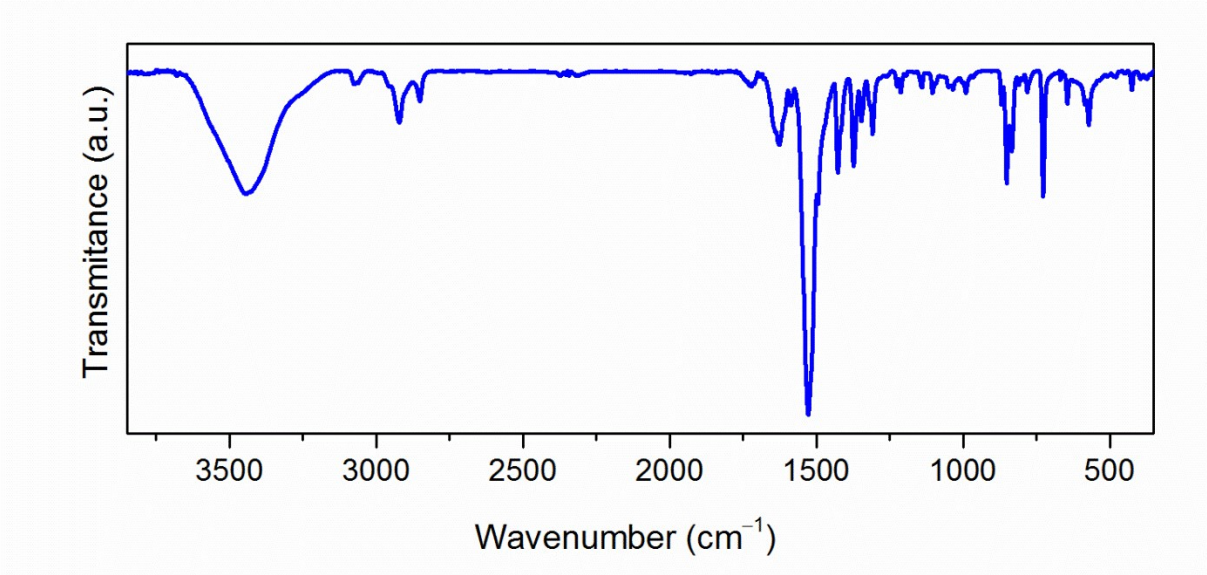

Figure S8 IR spectrum of the compound **1**.

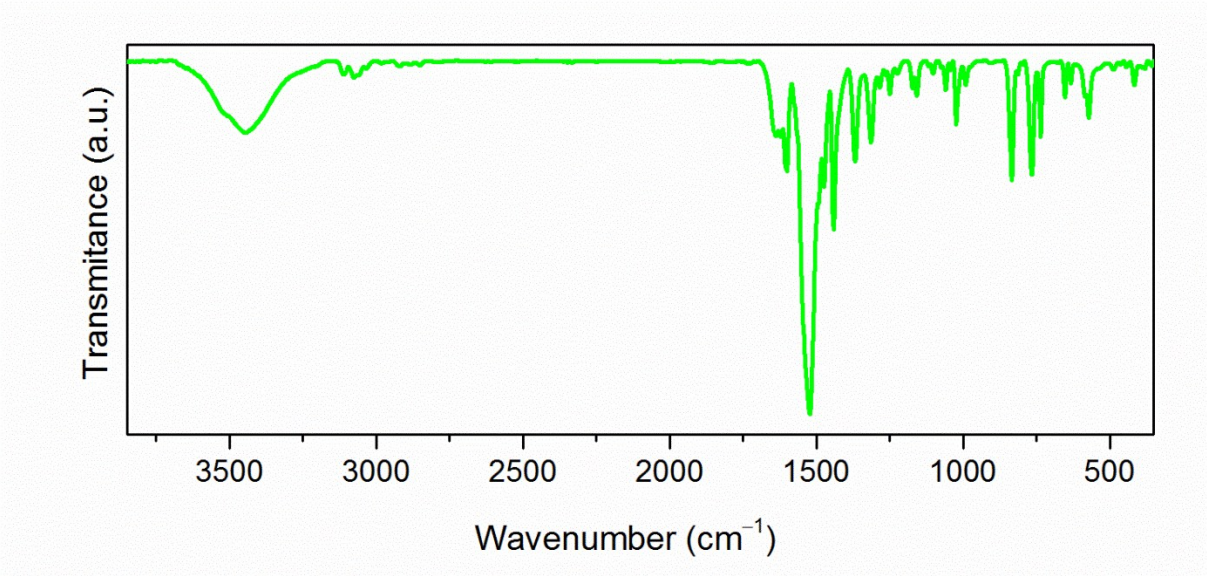

Figure S9 IR spectrum of the compound **2**.

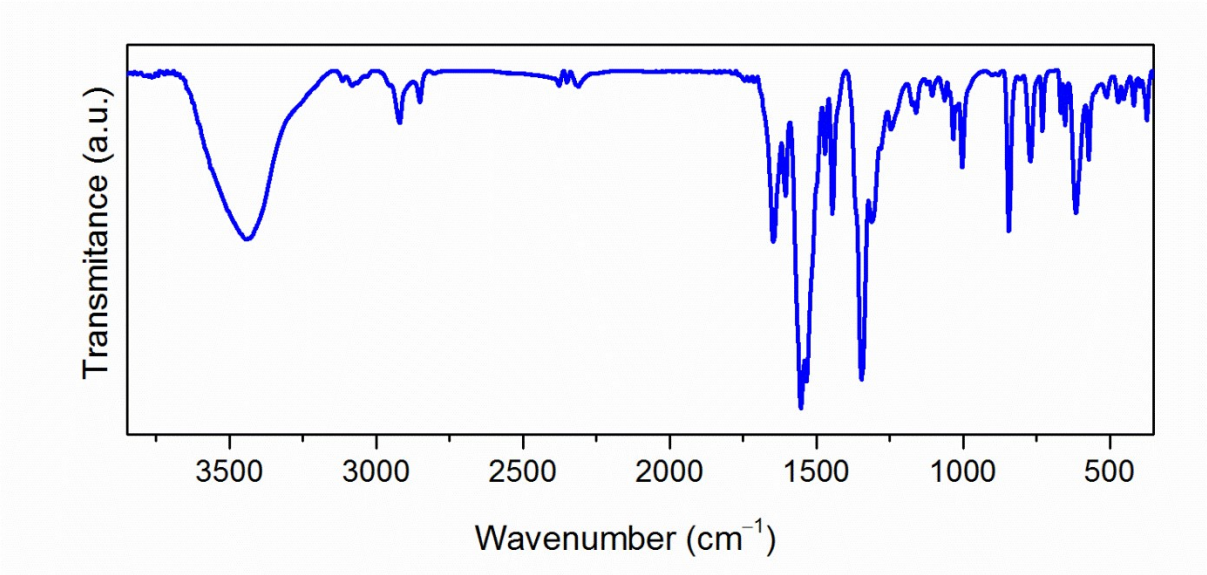

Figure S10 IR spectrum of the compound **3**.

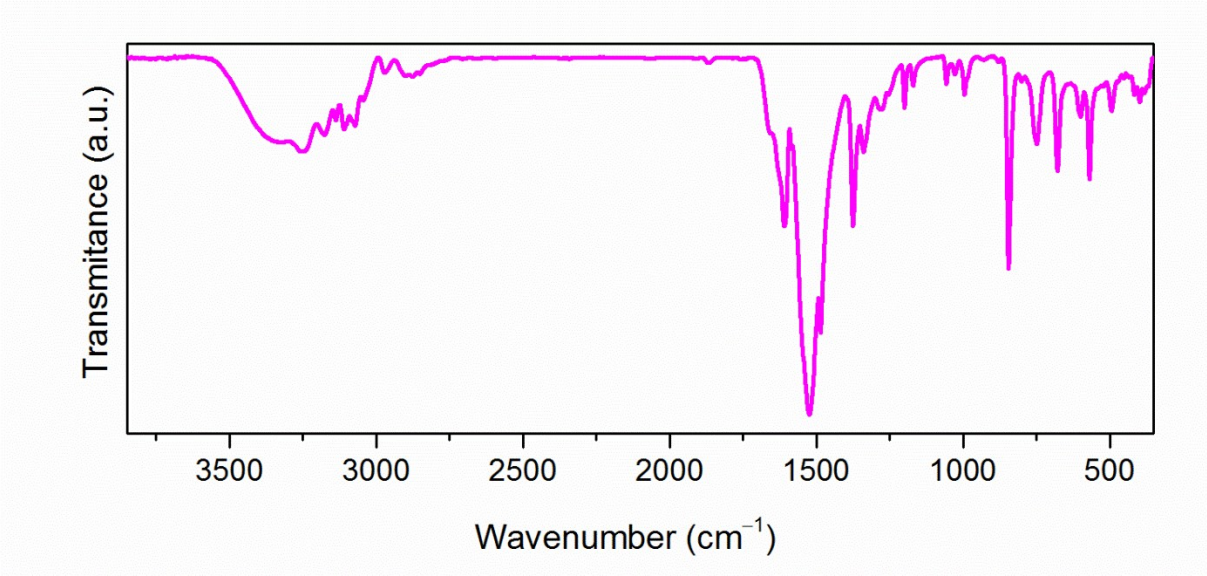

Figure S11 IR spectrum of the compound **4**.

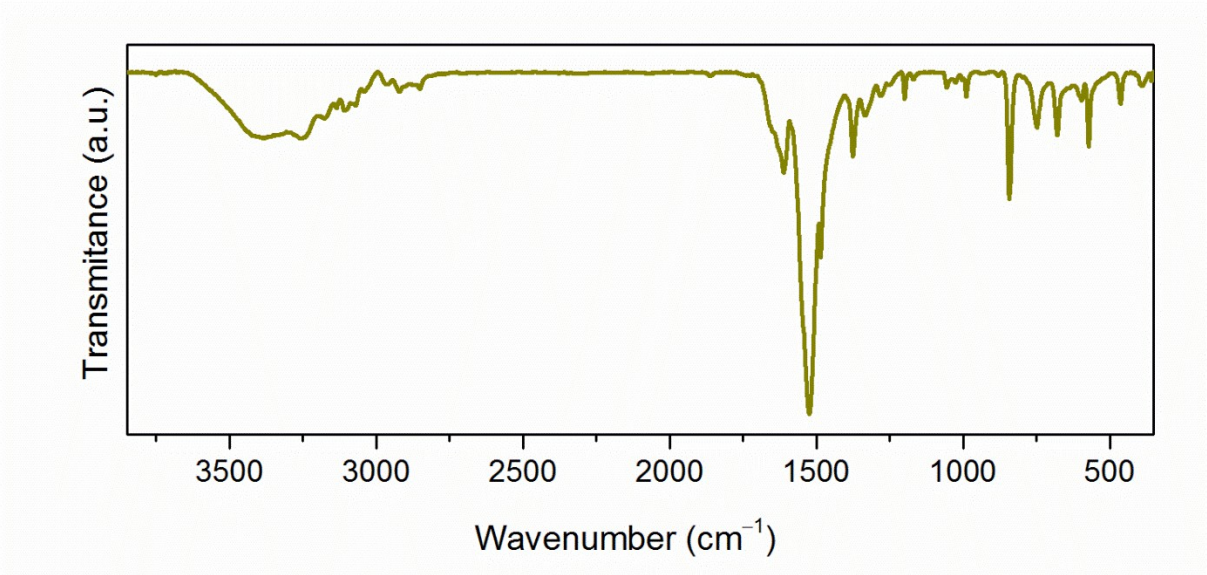

Figure S12 IR spectrum of the compound **5**.

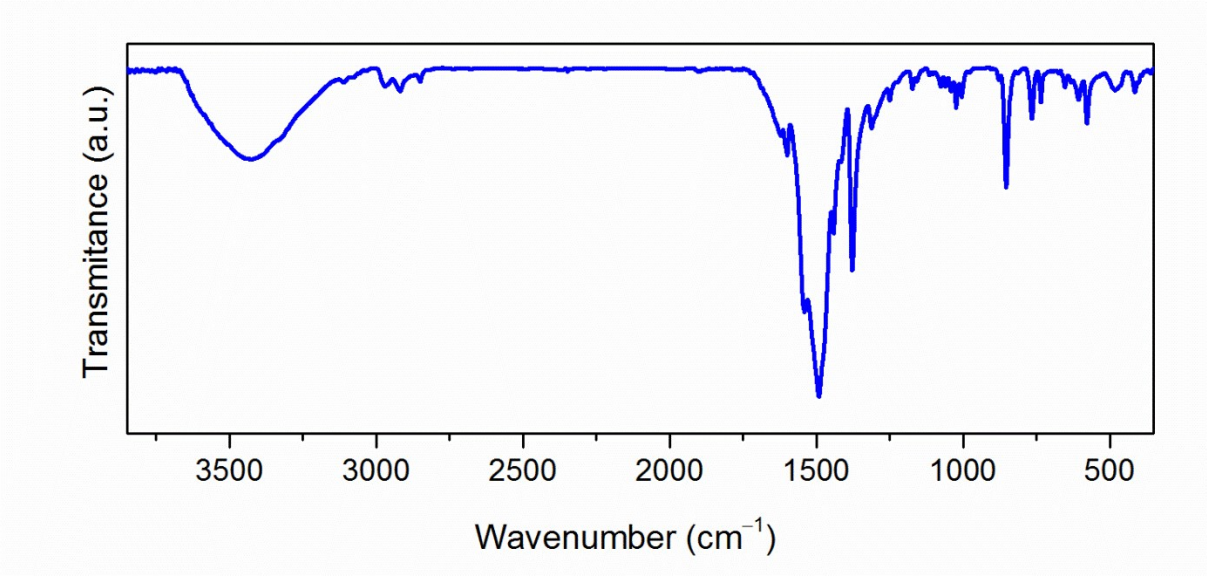

Figure S13 IR spectrum of the compound **6**.

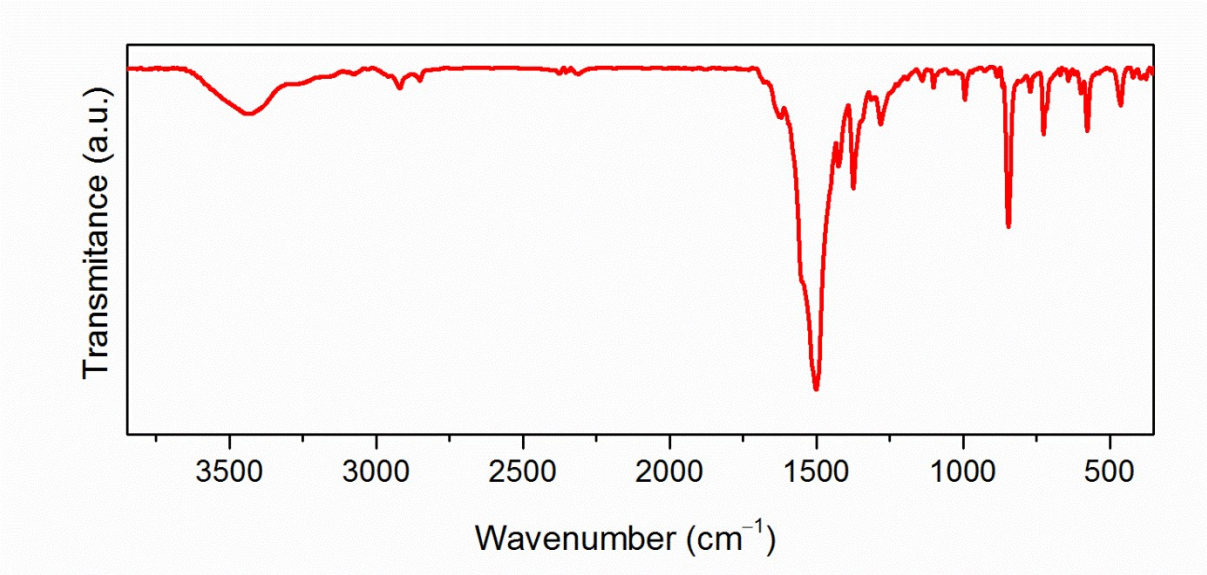

Figure S14 IR spectrum of the compound **7**.

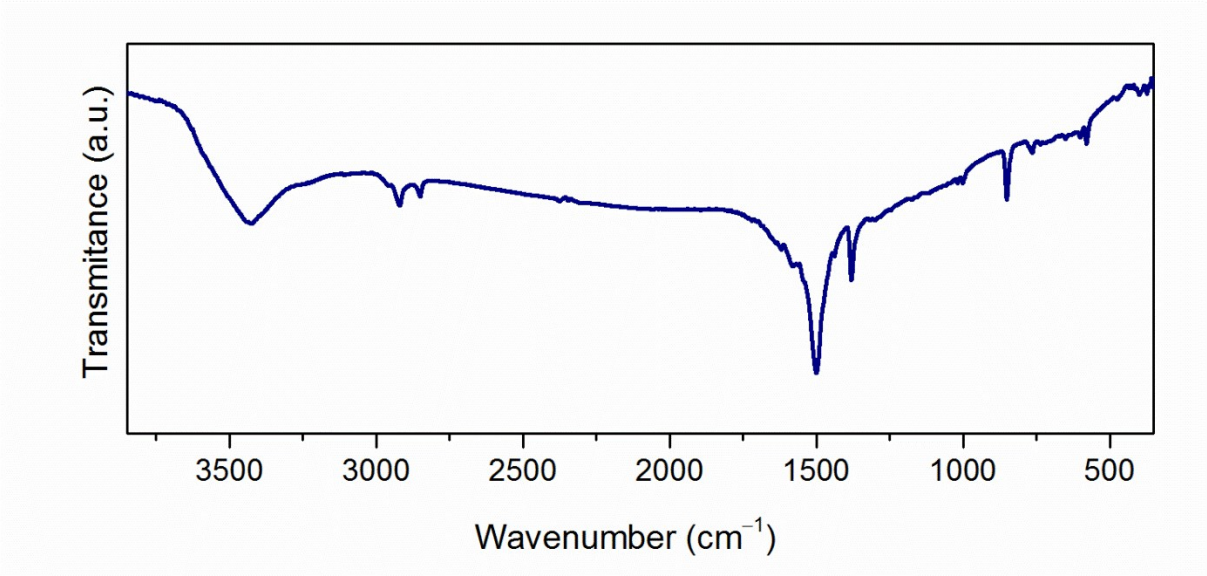

Figure S15 IR spectrum of the compound **8**.

References

[1] L. J. Farrugia, *J. Appl. Cryst.*, 1997, **30**, 565.

[2] A. Carrington, A. D. McLachlan, *Introduction to Magnetic Resonance*, Harper&Row, New York, 1967.

[3] C. Ruiz-Perez, P.A.L. Luis, F. Lloret, M. Julve, *Inorg. Chim. Acta* **336** (2002) 131–136.

[4] M. Jurić, P. Planinić, D. Žilić, B. Rakvin, B. Prugovečki, D. Matković-Čalogović, *J. Mol. Struct*. 924-926 (2009) 73-80.

[5] A. Bencini, D. Gatteschi, *Electron Paramagnetic Resonance of Exchange Coupled Systems*, Springer-Verlag, Berlin Heidelberg, 1990.

[6] N.Novosel, D. Žilić, D. Pajić, M. Jurić, B. Perić, K. Zadro, B. Rakvin, P. Planinić, Solid State Sci. 10 (2008) 1387-1394.

[7] D. Žilić, L. Androš, Y. Krupskaya, V. Kataev, B. Büchner, Appl. Magn. Reson. 46 (2015) 309-321.

[8] S. Stoll, A. Schweiger, J. Magn. Reson. 178 (2006) 42.

[9] A. Abragam and B. Bleaney, Electron Paramagnetic Resonance of Transition Ions, Clarendon Press, Oxford, UK, 1970.

[10] R. Bogumil, R. Kappl, J. Hüttermann, C, Sudfeldt, H. Witzel, Eur. J. Biochem. 213 (1993) 1185-1192.

[11] D. Deguenon, G. Bernardinelli, J. P. Tuchagues, P. Castan, Inorg. Chem. 29 (1990) 3031–3037.

[12] M. Jurić, D. Pajić, D. Žilić, B. Rakvin, K. Molčanov, J. Popović, Dalton Trans. 44 (2015) 20626.